Chinese Journal of Chemical Engineering 85 (2025) 206–216

Contents lists available at ScienceDirect

Chinese Journal of Chemical Engineering

journal homepage: www.elsevier.com/locate/CJChE

Full Length Article

Study of defluorination by thermal treatment of phosphogypsum under steam atmosphere

Huagui Jin [1, #], Xuebin An [2, #], Shizhao Wang [1], Yunshan Wang [2, *], Gang Yang [2, *], Yong Sun [3]

[1] School of Chemical Engineering and Technology, Hebei University of Technology, Tianjin 300130, China
[2] National Engineering Research Center of Green Recycling for Strategic Metal Resources, Chinese Academy of Sciences, Beijing 100190, China
[3] Department of Chemical and Environmental Engineering, University of Nottingham Ningbo China, Ningbo 315100, China

ARTICLE INFO

Article history:
Received 30 October 2024
Received in revised form
15 January 2025
Accepted 20 February 2025
Available online 17 March 2025

Keywords:
Phosphogypsum
Defluorination
High-temperature hydrolysis
Steam
Silica
Kinetics

ABSTRACT

This study investigates the removal of fluorine (F) impurities from phosphogypsum (PG) using steam as the reaction medium. The effects of the reaction atmosphere, temperature, time, and steam velocity on F impurities removal were systematically examined. The results showed that with a steam velocity of 0.0184 $m \cdot s^{-1}$, a reaction temperature of 700 °C, and a reaction time of 60 min, the F removal rate reached 95.87%. Further investigations into the defluorination mechanism revealed that steam and SiO_2 synergistically enhance fluoride removal, playing a crucial role in improving the defluorination efficiency. Kinetic analysis of the defluorination process, based on the shrinking core model (SCM), indicated that internal diffusion is the rate-controlling step, with the activation energy of 30.12 $kJ \cdot mol^{-1}$. This study identifies optimal conditions for PG defluorination and proposes a defluorination mechanism, contributing to the theoretical understanding of impurity removal through the thermal treatment of PG.

1. Introduction

Phosphogypsum (PG), a byproduct of the wet-process phosphoric acid production, primarily consists of dihydrate calcium sulfate ($CaSO_4 \cdot 2H_2O$) and contains various impurities, including phosphorus (P), silicon (Si), and fluorine (F). With the rapid development of the phosphate fertilizer industry in China, PG production has increased annually, reaching 80 million tons per year, with a cumulative stockpile of approximately 600 million tons [1–3]. However, the comprehensive utilization rate of PG remains below 46%. The primary cause of this low utilization is the presence of impurities, particularly harmful fluorine (F), which not only reduces the quality and value of PG products but also poses environmental risks. Furthermore, fluorine, a valuable strategic resource, accounts for approximately 800000 tons (calculated at 1%(mass)) in the annual production of PG, representing 40% of annual fluorine consumption in China. Recovering fluorine from PG could significantly enhance PG quality, conserve fluorine resources, reduce environmental risks, and promote the sustainable development of the phosphorus chemical industry.

To date, numerous scholars have researched the composition, occurrence [4–6] and removal methods [7–9] of fluorine in PG. The composition and occurrence of fluorine impurities in PG can vary slightly depending on the source of phosphate rock and the processing methods used. Zhao *et al.* [5] analyzed the composition and relative content of fluorine in PG, revealing that potassium fluosilicate (K_2SiF_6) and sodium fluosilicate (Na_2SiF_6) constitute relatively high proportions, with a combined content of 41.52%. In contrast, calcium fluoride (CaF_2) represents a smaller proportion, with a relative content of 3.62%. Li *et al.* [6] employed X-ray photoelectron spectroscopy (XPS) peak fitting to analyze fluorine compounds in PG, concluding that fluorides are predominantly present as K_2SiF_6 and Na_2SiF_6. Further analysis using electron backscatter diffraction-energy dispersive X-ray spectroscopy (EBSD-EDS) revealed that CaF_2 is adsorbed on the surface of $CaSO_4 \cdot 2H_2O$ crystals. Additionally, Na_2SiF_6 exists in combined with K_2SiF_6, while part of K_2SiF_6 is associated with $CaSO_4 \cdot 2H_2O$, and another portion exists independently [7–18].

To investigate the effects of various treatment methods on the defluorination of PG, Table 1 summarizes the principal techniques, including water washing, screening, acid treatment, lime neutralization, and thermal treatment methods. These methods are

* Corresponding authors.
E-mail addresses: wangys@ipe.ac.cn (Y. Wang), yanggang@ipe.ac.cn (G. Yang).
# These two authors contribute equally to this work.

https://doi.org/10.1016/j.cjche.2025.02.018

Table 1
Comparison of different defluorination methods for PG, SWP refers to secondary water pollution.

Methods	Defluorination rate/%	Pollution	Energy consumption (Cost)	Reference
Water washing	About 50%	SWP	High	[11–13]
Screening	<30%	None	Low	[10]
Acid treatment	>90%	SWP	High	[14]
Lime neutralization	About 50%	Minor	Low	[11,15]
Thermal treatment	>90%	Minor	High	[13,19]

evaluated based on defluorination rate, energy consumption/cost, and pollution impact. As indicated in Table 1, acid treatment (sulfuric acid method) and thermal treatment methods achieve defluorination rates exceeding 90% [16], demonstrating high efficiency. However, these methods are costly, and acid treatment may cause secondary water pollution [18]. Water washing and lime neutralization effectively remove soluble fluorine, with defluorination rates around 50%, but their efficiency in removing insoluble fluorine is limited [14,17]. Screening, with a defluorination efficiency typically below 30%, is highly dependent on particle size and density. Overall, thermal treatment provides significant advantages in defluorination efficiency and pollution control. Additionally, it can convert $CaSO_4 \cdot 2H_2O$ in PG into anhydrous calcium sulfate ($CaSO_4$), a product with broad application prospects in the construction industry.

The key conditions for the thermal treatment method for removing fluorine impurities from PG are the reaction temperature and atmosphere. Studies have shown that the fluorine removal rate is positively correlated with the reaction temperature. For example, Ren *et al.* [9,19,20] studied fluorine removal rates from PG at temperatures of 700 °C, 800 °C and 950 °C, achieving removal rates of 64.97%, 85.27%, and 93.89%, respectively. Additionally, the reaction atmosphere also significantly impacts the defluorination process. Pan *et al.*[21] studied the decomposition of Na_2SiF_6 in a nitrogen (N_2(g)) atmosphere. The results showed that when the temperature reached 700 °C and the reaction was sustained for 60 min, 99.6% of Na_2SiF_6 decomposed, producing NaF and gaseous silicon tetrafluoride (SiF_4(g)). Additionally, it was also observed that a molten layer (NaF-Na_2SiF_6) formed during the reaction, which hindered the diffusion of SiF_4(g) [21–23]. Stodolski *et al.* [24] studied the decomposition of K_2SiF_6 under steam conditions and finding that steam significantly enhanced fluoride removal. When the temperature was in the range of 400–500 °C, H_2O reacted with K_2SiF_6 to produce K_2SiO_3. Furthermore, under steam conditions, SiO_2 significantly improved the removal efficiency of halogenated compounds. Liu *et al.* [25,26] found that SiO_2 could promote the high-temperature hydrolysis of calcium chloride ($CaCl_2$) by weakening the Ca-Cl bond, which lowered the reaction energy barrier and ultimately produced calcium silicate ($CaSiO_3$). In summary, the reaction temperature and atmosphere have a significant impact on the removal efficiency of F impurities in PG, while the presence of silica (SiO_2) in PG also influences the removal of halogens. However, the existing literature on the thermal treatment methods for the removal of fluorine impurities from PG is relatively limited, and there is a noticeable gap in the studies regarding the relevant mechanisms, principles, and the kinetics of defluorination. Based on this, this study undertakes the following research.

Firstly, the removal of fluorine from PG under different reaction conditions was investigated, focusing on the effects of reaction temperature and atmosphere (N_2(g), H_2O(g), CO_2(g)) on the defluorination rate of PG, while analyzing the changes in the composition of fluorine in PG during the reaction process. Secondly, a kinetic study of defluorination in PG was conducted, concentrating on the defluorination process of PG in a steam atmosphere to analyze and identify the controlling steps of the defluorination reaction. Finally, the defluorination mechanism of PG under the influence of steam was explored. The research presented in this paper will provide practical pathways and theoretical support for the defluorination and resource utilization of PG.

2. Experimental

2.1. Experimental materials

The PG samples were obtained from Hubei Xingfa Chemical Group Co., Ltd. in Yichang, Hubei Province, with a water content of 18.9%. Fig. 1 and Table 2 show the analysis of the phase composition and chemical elements of PG using XRD, XPS, SEM, EDS, and XRF. The results indicate that the primary phases of PG are $CaSO_4 \cdot 2H_2O$ and SiO_2, and its chemical composition contains elements such as Ca, S, Si, P and F.

The chemical reagents used in the experiments included $CaSO_4 \cdot 2H_2O$ (≥99.0%, Sinopharm Chemical Reagent Co., Ltd.), K_2SiF_6 (99.0%, Aladdin), Na_2SiF_6 (98.0%, Aladdin), CaF_2 (99.0%, Aladdin), and SiO_2 (≥97.0%, Xilong Scientific Co., Ltd.).

The water used for the experiments was deionized water.

As shown in Fig. 1(a), XRD has limitations in analyzing the fluorine composition in PG, as no characteristic peaks for fluorine compounds were detected. To address this issue, Electron back scatter diffraction-energy dispersive spectroscopy (EBSD-EDS), along with X-ray photoelectron spectroscopy (XPS), were employed to analyze the composition, occurrence state, and relative content of fluorine in PG. The EBSD-EDS analysis presented in Fig. 2(a)–(b) indicates that the fluorides present in PG include CaF_2, Na_2SiF_6, and K_2SiF_6. Specifically, CaF_2 is found adsorbed on the surface of $CaSO_4 \cdot 2H_2O$ crystals. Additionally, a portion of K_2SiF_6 forms complexes with Na_2SiF_6, while another part exists as independent particles. To achieve a more precise quantification of the different fluoride contents in PG, XPS analysis of the fluorine element in PG was conducted. Fig. 2(c) presents the deconvolution of the characteristic peaks for the F 1s region in PG, where the F 1s spectrum exhibits three distinct peaks located at 686.6 eV, 686.0 eV, and 684.6 eV. By comparing these peaks with the NIST XPS database, it was found that the peak at 686.6 eV corresponds to K_2SiF_6, while the peaks at 686.0 eV and 684.6 eV correspond to Na_2SiF_6 and CaF_2, respectively. Based on the areas of the peaks shown in Fig. 2(c), the relative content of fluorine in PG's fluoride compounds can be quantified as K_2SiF_6: Na_2SiF_6: CaF_2 = 60: 35: 5.

2.2. Experimental process

The experimental apparatus is illustrated in Fig. 3. Initially, the gases required for the reaction atmosphere (H_2O(g), N_2(g), or CO_2(g)) are introduced into a preheating device with an inner diameter of 0.05 m for superheating. The superheated gases are subsequently transported through insulated piping into the tubular reactor. Subsequently, the ground and sieved PG powder (with a particle size of less than 125 μm) is placed into a corundum boat, which is positioned at the center of the tubular reactor that has been preheated to the specified temperatures (from 500 °C to

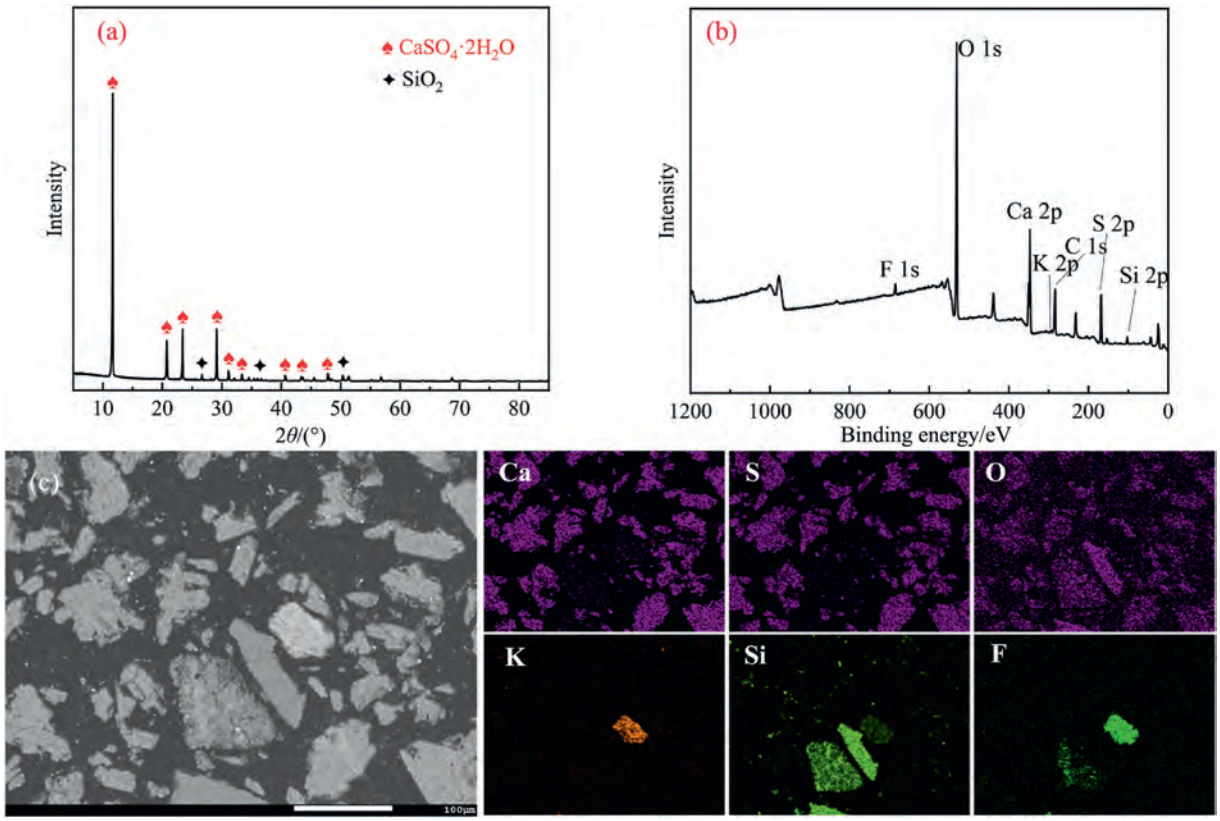

Fig. 1. Characterization of PG: (a) XRD analysis of PG, (b) XPS analysis of PG, (c) SEM-EDS mapping analysis of PG.

Table 2
Chemical composition of PG determined by XRF.

	SO_3	CaO	SiO_2	F	P_2O_5	K_2O	Fe_2O_3	Na_2O	Other
Content/%(mass)	45.809	4.032	8.021	0.810	0.593	0.520	0.408	0.131	0.676

800 °C) and maintained for a predetermined duration. Upon completion of the experiment, the corundum boat is removed from the reactor, and the fluorine content in the solid product is measured to calculate the defluorination rate. In addition, the gas generated during the reaction process is absorbed by the sodium hydroxide solution.

The defluorination rate (α, %) of fluorine in PG [27] is calculated as shown in Eq. (1):

$$\alpha = (M_1 - M_2) / M_1 \times 100\% \quad (1)$$

Where M_1 (g) represents the fluorine content in the PG feedstock, and M_2 (g) denotes the fluorine content in the product.

2.3. Analysis and characterization

X-ray fluorescence spectrometer (XRF) (PANalytical B.V., Netherlands) was used to determine the chemical composition.

X-ray diffractometry (XRD) (PANalytical B.V., Netherlands) was used to characterize the crystallite structure of the sample with detailed operational conditions setting as the following: graphite

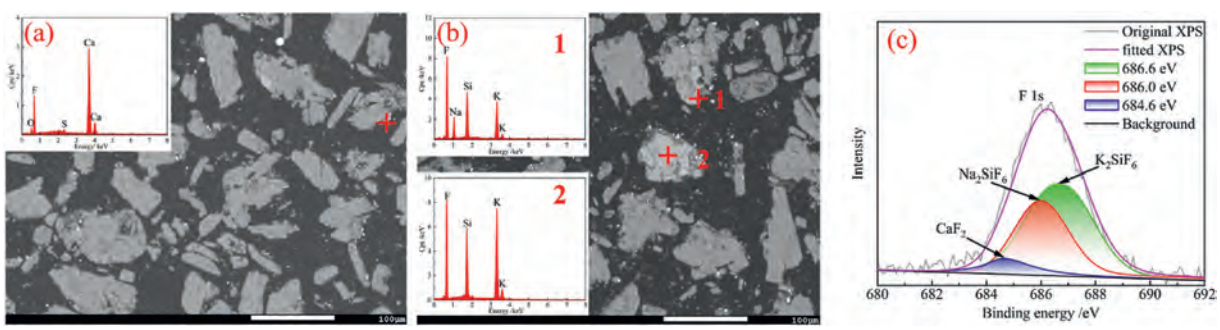

Fig. 2. EBSD-EDS and XPS analysis of PG: (a), (b) EBSD-EDS, (c) F 1s XPS spectra.

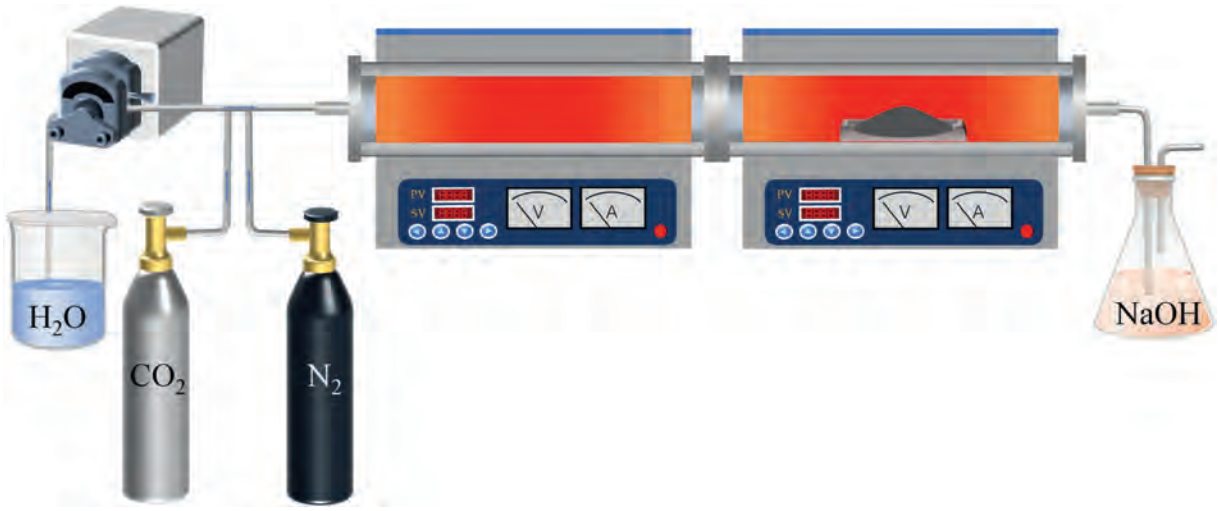

Fig. 3. Schematic diagram of the experimental setup.

filtered Cu K_α radiation, the acceleration voltage at 40 kV, the tube current at 30 mA, and the data are obtained in the scanning range of 5°–90° and the scanning time is 5.55 min.

The scanning electron microscope (SEM) (JSM-6700 F thermal field emission Scanning electron microscope) was used for the surface morphology (the accelerated voltage is 5 kV). Additionally, an electron backscatter diffraction (EBSD) system and X-ray energy dispersive spectrometry (EDS) were configured to analyze the elemental content and the relative distribution of elements within the samples.

X-ray photoelectron spectroscopy (XPS) (Thermo Fisher Scientific, Model ESCALAB 250Xi, Al K_α excitation source) was employed to analyze the elemental composition of the sample surfaces. The radiation source employed was Al K_α radiation, operating at a voltage of 12 kV and a current of 6 mA. Calibration was conducted using the C 1s peak of carbon impurities at 284.8 eV as the reference peak.

2.4. Thermodynamic analysis

The thermodynamic analysis of the potential reactions at equilibrium was performed by estimating the chemical potential or Gibbs free energy (ΔG) of the potential reactions using the HSC Chemistry 6.0 software. The Gibbs free energy is calculated as follows:

$$\Delta G = \Delta H - T\Delta S \quad (2)$$

Where ΔG (kJ·mol^{-1}) refers to the Gibbs free energy, ΔH (kJ·mol^{-1}) refers to the enthalpy, ΔS (kJ·mol^{-1}) refers to the entropy, and T (K) refers to temperature of investigated system.

3. Results and Discussion

3.1. Thermodynamic analysis of the potential reaction

The defluorination of PG via heat treatment is a complex process that involves multiple reaction pathways, including thermal decomposition, high-temperature hydrolysis, and volatilization. At elevated temperatures, fluosilicates in PG decompose into SiF_4, NaF, and KF. Due to the high melting and boiling points of CaF_2, KF, and NaF, along with their low volatility, the effect of fluoride volatilization can be considered negligible in this study. Table 3 presents the potential reactions between fluorides in PG and steam, along with the reactions potentially caused by the synergistic effects of SiO_2 and steam on the fluorides.

Table 3
Summary of potential reactions estimated by thermodynamic analysis.

Number	Reactions
R1	$Na_2SiF_6 = 2NaF + SiF_4(g)$
R2	$K_2SiF_6 = 2KF + SiF_4(g)$
R3	$4NaF + 3SiO_2 = 2Na_2SiO_3 + SiF_4(g)$
R4	$4KF + 3SiO_2 = 2K_2SiO_3 + SiF_4(g)$
R5	$2NaF + H_2O(g) = Na_2O + 2HF(g)$
R6	$2KF + H_2O(g) = K_2O + 2HF(g)$
R7	$2NaF + SiO_2 + H_2O(g) = Na_2SiO_3 + 2HF(g)$
R8	$2KF + SiO_2 + H_2O(g) = K_2SiO_3 + 2HF(g)$
R9	$Na_2SiF_6 + 3H_2O(g) = Na_2SiO_3 + 6HF(g)$
R10	$K_2SiF_6 + 3H_2O(g) = K_2SiO_3 + 6HF(g)$
R11	$CaF_2 + H_2O(g) = CaO + 2HF(g)$
R12	$CaF_2 + SiO_2 + H_2O(g) = CaSiO_3 + 2HF(g)$
R13	$SiF_{4(g)} + 2H_2O(g) = SiO_2 + 4HF(g)$

The changes in Gibbs free energy (ΔG) of the potential reactions are shown in Fig. 4. These reactions are classified into two main

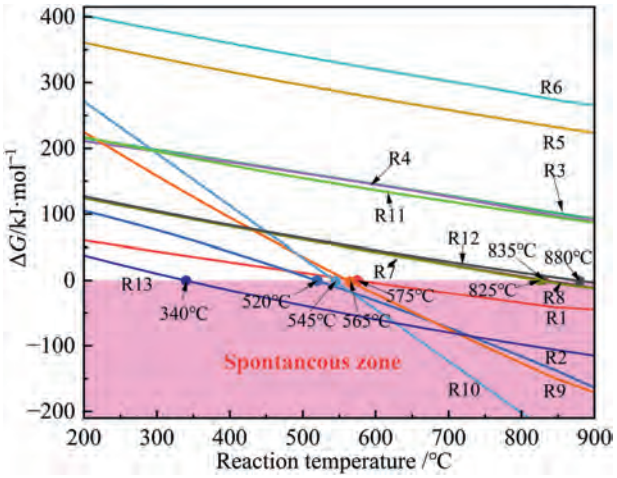

Fig. 4. Thermodynamic analysis of all potential reactions.

categories based on reaction conditions: (i) reactions without steam (R1–R4) and (ii) reactions with steam (R5–R13).

As shown in Fig. 4, the ΔG values for all reactions exhibit a decreasing trend with increasing temperature, indicating that a high-temperature environment favors the removal of fluorine. Specifically, reactions R1 and R2 correspond to the thermal decomposition of Na_2SiF_6 and K_2SiF_6, producing NaF, KF, and SiF_4, while reactions R9 and R10 represent high-temperature hydrolysis reactions, yielding Na_2SiO_3, K_2SiO_3, and HF. When the reaction temperatures exceed 575 °C, 520 °C, 565 °C and 545 °C, the ΔG for these four reactions enter the spontaneous zone. For the defluorination reactions of NaF and KF (R3–R8), comparing the effects of SiO_2 and steam on the reaction temperatures (R3–R6) shows that SiO_2 reduces the decomposition temperature of the fluorides more significantly than steam. In terms of ΔG changes, the driving forces for reactions R3 and R4 (with SiO_2 participating) are much smaller than those for reactions R7 and R8 (with both SiO_2 and steam participating). This indicates that the combined effect of steam and SiO_2 significantly reduces the energy barrier for NaF or KF defluorination. However, the reaction temperatures for R7 and R8 must reach at least 825 °C and 835 °C, respectively. Reactions R11 and R12 compare the thermodynamic analysis of the high-temperature hydrolysis of CaF_2 with and without SiO_2. It was found that in the simultaneous presence of SiO_2 and steam, the hydrolysis temperature of CaF_2 is lowered to 880 °C. In reaction R13, when the temperature reaches 340 °C, SiF_4(g) reacts with steam to form HF(g) and SiO_2.

Considering that the main fluoride in PG is fluorosilicate, thermodynamic calculations show that its minimum decomposition temperature is 520 °C. Moreover, Refs [21,24] and experimental results show that once the reaction temperature exceeds 700 °C, further temperature increases have little impact on fluoride removal from fluorosilicates. Thus, this study focuses on a temperature range of 500–700 °C for investigation. Within this range, the high-temperature hydrolysis reactions of NaF, KF and CaF_2 are non-spontaneously ($\Delta G>0$). Consequently, reactions R3–R8, R11, and R12 are excluded from this study.

In summary, within the studied temperature range, the possible reactions include R1, R2, R9, R10 and R13. During the defluorination process of PG, steam and SiO_2 play crucial roles, with their synergistic effect promoting the conversion of fluoride in the fluorides into easily volatile HF, thereby achieving effective removal of fluoride.

3.2. Effect of process parameters

3.2.1. Effect of reaction atmosphere and temperature

The effect of reaction temperature and atmosphere on the defluorination efficiency of PG is shown in Fig. 5. The study shows that under the same atmosphere, PG defluorination efficiency increases steadily with rising temperature. Upon introducing steam, the fluorine removal rate increased from 69.22% to 95.87%. In N_2(g) and CO_2(g) atmospheres, the fluorine removal rates increased from 31.24% to 32.40% to 61.65% and 59.67%, respectively. In addition, in a steam atmosphere, when the temperature exceeds 700 °C, the fluorine removal rate remains nearly constant, indicating equilibrium has been reached. The study suggests that the optimal reaction atmosphere for PG defluorination is a steam, with an ideal temperature of 700 °C.

3.2.2. Effect of reaction time

Fig. 6 shows the effect of reaction time on the fluorine removal from PG at a reaction temperature of 700 °C and a steam velocity of 0.0184 m·s^{-1}. As the reaction time increases, the defluorination rate of PG steadily increases. With a reaction time of 5 min, the fluorine removal rate reached 57.41%, which was due to the increase in temperature leading to the dehydration of $CaSO_4 \cdot 2H_2O$, the disruption of the crystal structure, and the formation of interstitial gaps between the $CaSO_4$ crystals. The formation of gaps enhanced mass transfer between the fluorine compounds and the gas phase, facilitating the more efficient release of SiF_4 or HF from the PG matrix. Increasing the reaction time to 60 min resulted in a fluorine removal rate of 95.87%. Beyond 60 min, the fluorine removal rate remained stable, indicating that 60 min is the optimal reaction time.

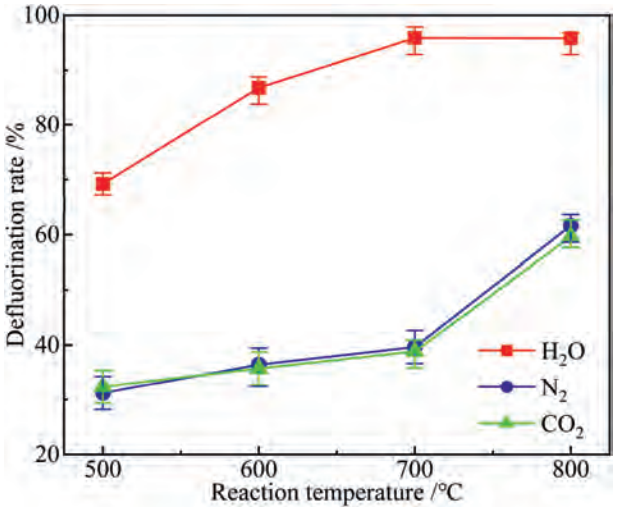

Fig. 5. Effect of reaction atmosphere and temperature on the defluorination of PG (N_2(g) = 1.6637 m·s^{-1}, CO_2(g) = 1.6637 m·s^{-1}, H_2O(g) = 0.0184 m·s^{-1}).

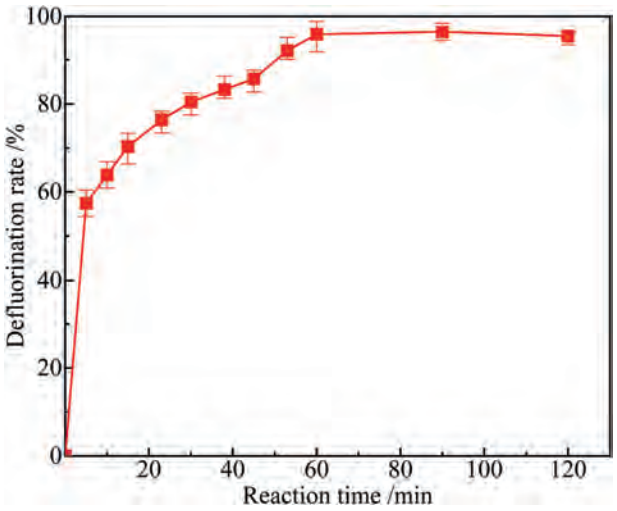

Fig. 6. Effect of reaction time on the defluorination of PG (700 °C, H_2O(g) = 0.0184 m·s^{-1}).

3.2.3. Effect of steam velocity

In this study, steam is used as the defluorination medium for PG, and its flow rate is quantified as steam velocity. Fig. 7 illustrates the effect of steam velocity on fluorine removal efficiency in PG under the reaction conditions of 700 °C and a duration of 60 min. As the steam velocity increases, the fluorine removal rate in PG steadily improves. When the steam velocity increases from 0 to 0.0184 m·s^{-1}, the fluorine removal rate rises from 39.65% to 95.87%. Notably, when the steam velocity is 0, the fluorine removal rate is only 39.65%. This results from the formation of KF, NaF, and SiF_4

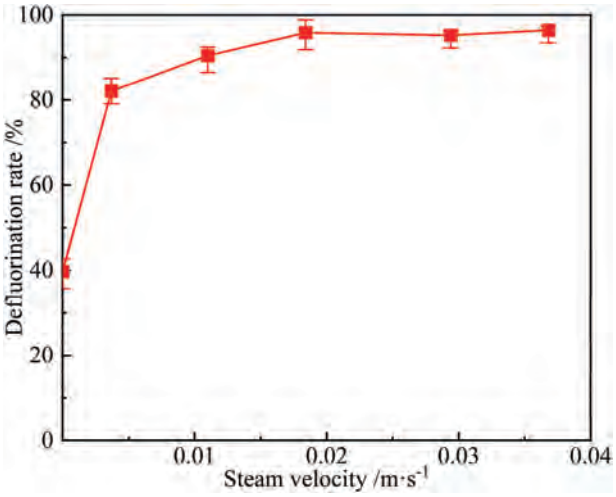

Fig. 7. Effect of steam velocity on the defluorination of PG (700 °C, 60 min).

from the fluorosilicates (K_2SiF_6 and Na_2SiF_6) in PG at high temperatures. KF and NaF react with the unreacted fluorosilicates to form a molten layer that hinders SiF_4 diffusion, resulting in a lower defluorination rate in PG [21,28]. As the steam velocity increases to 0.0184 m·s^{-1}, the fluorine removal rate in PG rises rapidly to 95.87%. This is due to the introduction of steam altering the reaction pathways of the fluorosilicates, shifting from reactions R1 and R2 to reactions R9 and R10, resulting in the formation of silicates and HF. This change in reaction pathways prevents molten layer formation, thereby significantly improving the fluorine removal rate in PG. The results indicate that the optimal steam velocity is 0.0184 m·s^{-1}.

3.3. Kinetic analysis

In this work, the shrinking core model (SCM) is used to estimate the defluorination process of PG [29,30]. As shown in Fig. 8(a)–(d), the defluorination reaction of PG is typically controlled by the following steps: (a) external diffusion control, (b) internal diffusion control, (c) chemical reaction control, and (d) diffusion-chemical reaction control. Under different control conditions, the kinetic equations are as follows in Eqs. (3)–(6):

External diffusion as a controlling step:

$$kt = \alpha \tag{3}$$

Internal diffusion as a controlling step:

$$kt = 1 + 2(1-\alpha) - 3(1-\alpha)^{2/3} \tag{4}$$

Chemical reaction as a controlling step:

$$kt = 1 - (1-\alpha)^{1/3} \tag{5}$$

Diffusion-chemical reaction as a controlling step:

$$kt = (1/3)\ln(1-\alpha) - 1 + (1-\alpha)^{-1/3} \tag{6}$$

Where t (min) represents the reaction time, α (%) is the fluoride removal rate, and k (min^{-1}) is the apparent rate constant.

The kinetic results of PG defluorination in a steam atmosphere at three different temperatures (from 500°C to 700 °C) are shown in Fig. 8. The correlation coefficients R^2 indicate that (external diffusion control, R^2 = 0.9478; internal diffusion control, R^2 = 0.9908; chemical reaction control, R^2 = 0.9786; diffusion-chemical reaction control, R^2 = 0.9295), with internal diffusion showing the best linear fitting performance as the controlling step. In the process of defluorination of PG in a steam atmosphere, internal diffusion significantly influences the decomposition of fluorides, and the corresponding regression apparent rate constants k are summarized in Fig. 8(b).

The activation energy of the reaction is described using the Arrhenius equation and its logarithmic form (Eq. (7)–(8)), which describes the relationship between the reaction rate constant k(min^{-1}) and temperature T(K).

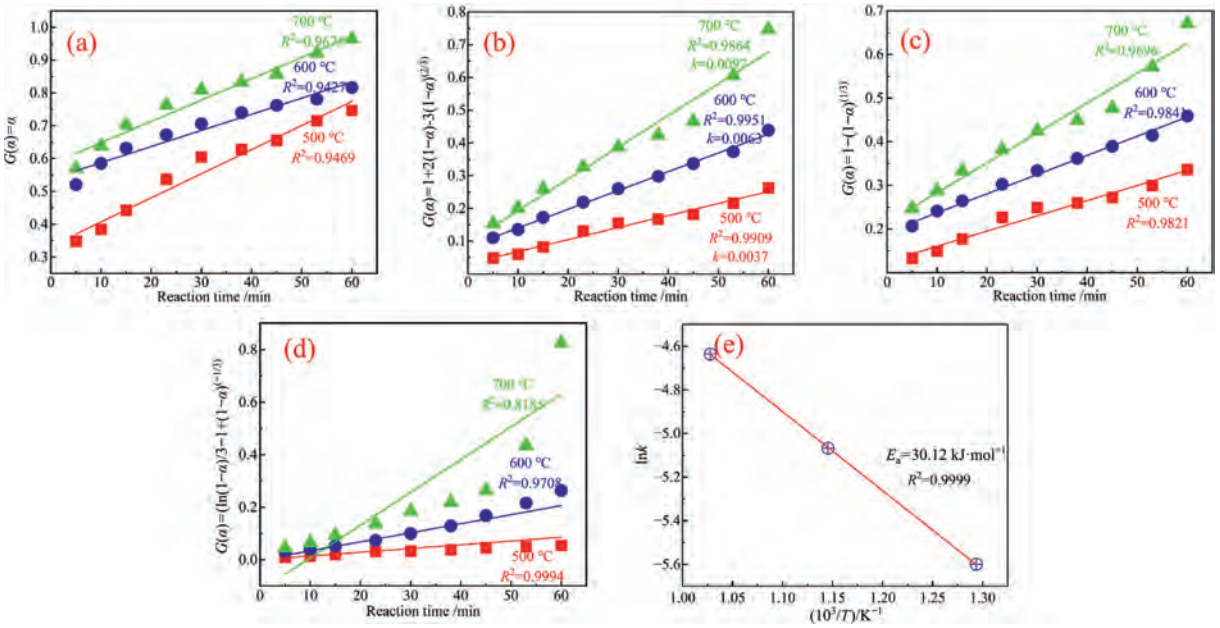

Fig. 8. Kinetics of PG defluorination using SCM at different temperatures: (a) curve fitting using the external diffusion control model, (b) curve fitting using the internal diffusion control model, (c) curve fitting using the chemical reaction control model, (d) curve fitting using the reaction-diffusion control model, (e) activation energy estimation.

$$k = A_0 \exp(-E_a/RT) \quad (7)$$

$$\ln k = \ln A_0 - E_a/RT \quad (8)$$

where A_0 is the pre-exponential factor (min^{-1}), R (8.314 J·mol^{-1}·K^{-1}) is the ideal gas constant, and E_a (kJ·mol^{-1}) is the activation energy. As shown in Fig. 8(e), the activation energy (E_a) for the defluorination of PG in a steam atmosphere is 30.12 kJ·mol^{-1}. Previous studies have shown [23,28,31] that the activation energy (E_a) of the fluoride defluorination reaction in non-steam atmospheres generally ranges from 61.35 to 182 kJ·mol^{-1}. These results suggest that steam atmospheres can significantly reduce the activation energy of PG defluorination, making it more efficient.

3.4. Mechanism of fluorine impurities removal from PG

According to literature reports [25,30], the synergistic effect of silica and steam at high temperatures promotes the decomposition of halogenated compounds. To further investigate whether the presence of SiO_2 in PG facilitates defluorination, mixtures were prepared using analytically pure chemical reagents. These mixtures were formulated according to the main components and ratios of $CaSO_4·2H_2O$, SiO_2, and fluorides (CaF_2, Na_2SiF_6, K_2SiF_6) found in PG. These mixtures, both with and without SiO_2, were prepared, and the experimental steps described in Section 2.2 were followed. The study focused on two main aspects to reveal the defluorination mechanism: (i) exploring the effect of SiO_2 on the high-temperature hydrolysis of fluorine-containing mixtures, and (ii) characterizing and analyzing changes in fluorine composition in the solid-phase products.

3.4.1. Effect of SiO_2 on defluorination of fluorinated mixtures

The results of the process experiments indicated that the optimal conditions for the defluorination of PG were as follows: steam as the reaction atmosphere, the steam velocity of 0.0184 m·s^{-1}, the reaction temperature of 700 °C, and the reaction time of 60 min.

Fig. 9(a)–(d) illustrates the effect of SiO_2 on the defluorination of $CaSO_4·2H_2O$ containing fluoride under optimal process conditions. As shown in Fig. 9(a)–(d), comparing the defluorination rate curves with and without SiO_2 reveals that the addition of SiO_2 significantly enhances defluorination efficiency. Fig. 9(a) and (b) indicate that the defluorination rate of K_2SiF_6 is slightly higher than that of Na_2SiF_6, which is consistent with our previous conclusions from density functional theory (DFT) calculations, showing that compounds with higher total energy of fluorides are more susceptible to hydrolysis. The calculated total energies of CaF_2, Na_2SiF_6, and K_2SiF_6 are 35.776, 120.130, and 216.102 kJ·mol^{-1}·atom^{-1}, respectively [10]. As shown in Fig. 9(a)–(c), the defluorination rate of $CaSO_4·2H_2O$ containing fluorosilicates is slightly higher than that of

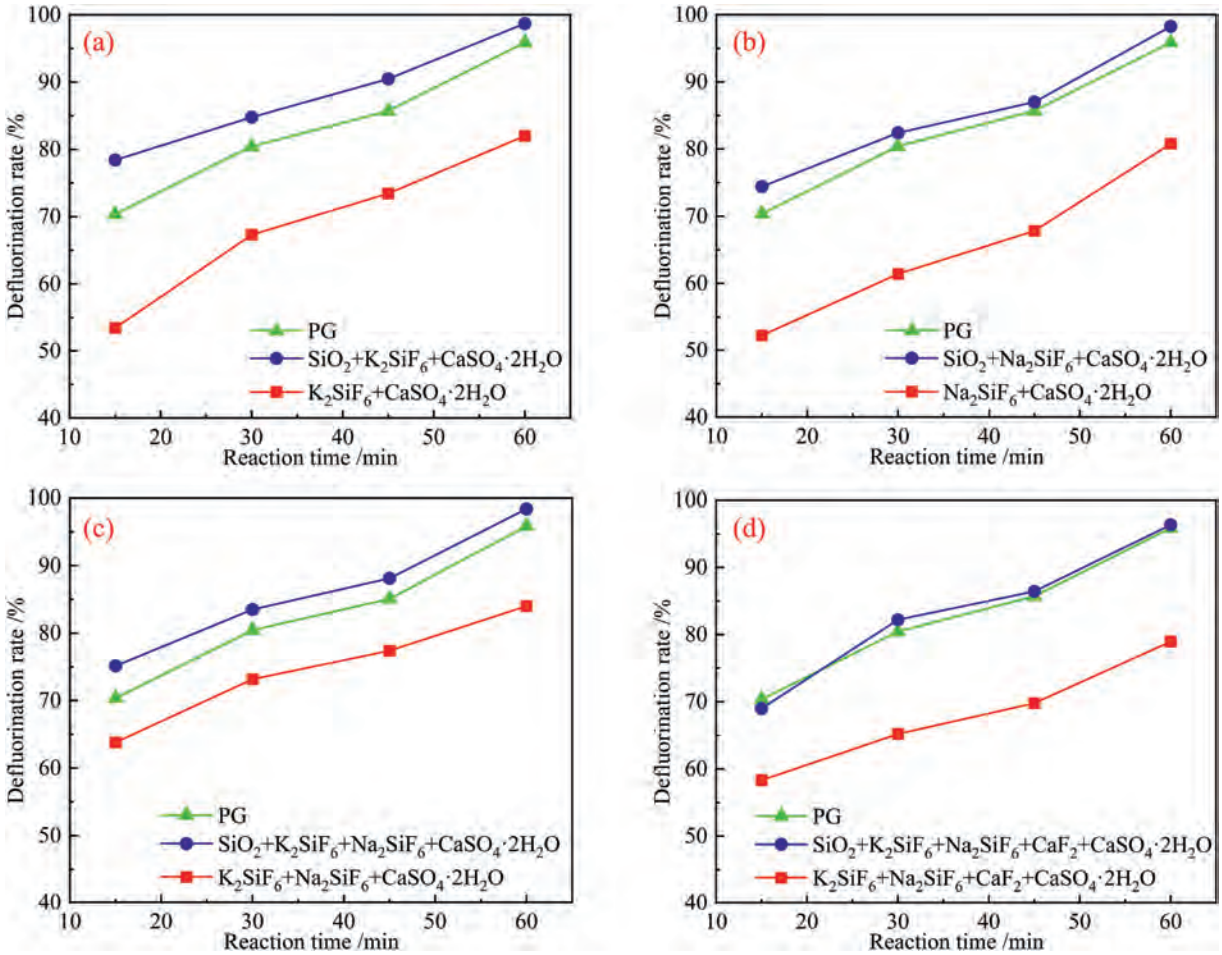

Fig. 9. Effect of SiO_2 on the defluorination of fluorine compounds: (a) $CaSO_4·2H_2O$ + K_2SiF_6, (b) $CaSO_4·2H_2O$ + Na_2SiF_6, (c) $CaSO_4·2H_2O$ + K_2SiF_6+Na_2SiF_6, (d) $CaSO_4·2H_2O$ + K_2SiF_6+Na_2SiF_6+CaF_2.

PG. This is attributed to the presence of CaF_2 in PG, which is more difficult to hydrolyze [32,33]. As shown in Fig. 9(d), with the addition of SiO_2 and CaF_2, the defluorination rate approaches that of the fluorine removal rate in PG, further confirming the previous analysis of the composition of fluorides in PG. Studies indicate that the addition of SiO_2 to PG facilitates the fluorine removal, with K_2SiF_6 being the easiest to remove, followed by Na_2SiF_6, while CaF_2 is the most difficult to remove.

3.4.2. Investigation of defluorination of PG in steam atmosphere

Fig. 10(a)–(c) show the EBSD-EDS and XPS analysis results of the products obtained after 15 min of reaction. In Fig. 10(a)–(b), numerous cracks in the morphology of PG are clearly visible. This phenomenon is attributed to the dehydration of PG at high temperature, resulting in the transformation of $CaSO_4 \cdot 2H_2O$ crystals to $CaSO_4$ crystals. EBSD-EDS point scanning analysis in Fig. 10(a) shows that the atomic ratios of O, F, Na, Si and K in the product are approximately 3:24:1:5:9. Based on this observation, it can be inferred that the product contains both fluorosilicate and silicate. Fig. 10(b) provides specific EBSD-EDS analysis results for two points: Point 1, located at the particle edge, has an atomic ratio of K, Ca, Si, S, F and O of approximately 5:5:17:5:6:55, suggesting that Point 1 is composed of SiO_2, K_2SiO_3, K_2SiF_6, and $CaSO_4$. Point 2, located within the particle, has an atomic ratio of K, Si, and F of approximately 2:1:6, indicating that the chemical composition of Point 2 is K_2SiF_6. The analyses in Fig. 10(a) and (b) demonstrate that, in the presence of steam, K_2SiF_6 and Na_2SiF_6 in PG reacted to produce silicates (*e.g.,* Na_2SiO_3 and K_2SiO_3) as well as HF, while the generated K_2SiO_3, along with the original $CaSO_4$, encapsulated the unreacted K_2SiF_6.

To validate the aforementioned analytical results, XPS analysis was performed on the products following a 15 min reaction period (Fig. 10(c)). The results showed that the peak area of Na_2SiF_6 was greater than that of CaF_2 and K_2SiF_6. Compared to the XPS analysis of the PG raw materials (Fig. 2(d)), the peak area of K_2SiF_6 decreased significantly, indicating that K_2SiF_6 was preferentially decomposed during the initial stage of the reaction. This observation is consistent with the thermodynamic analysis of the high-temperature hydrolysis of Na_2SiF_6 and K_2SiF_6 presented in Fig. 4.

Fig. 11 illustrates the fluorine composition of the products obtained after a 45 min reaction in a steam atmosphere, analyzed using EBSD-EDS point scan and XPS techniques. Fig. 11(a) shows that the atomic ratios of O, Si and K in the products are approximately 30:14:3. Based on these ratios, it can be inferred that the products contain K_2SiO_3 and SiO_2. Fig. 11(b), indicates that the fluorides present in the products are primarily CaF_2 and Na_2SiF_6, while the characteristic peak of K_2SiF_6 is absent, suggesting the decomposition of K_2SiF_6 into K_2SiO_3 in presence of steam atmosphere.

As the reaction time is extended to 60 min, the fluoride removal rate in the PG reaches 95.87%. Fig. 12 shows that EBSD-EDS point scan analysis reveals the adsorption of CaF_2 on the surface of $CaSO_4$. XPS analysis of fluoride in PG was performed, and peak deconvolution of the XPS spectra indicated that the remaining fluoride species present in PG at this stage is CaF_2. This suggests that only CaF_2 remained while other types of fluoride contained compounds have been converted or removed.

By analyzing the changes in the binding energies of Si, K, and Na in PG before and after the reaction, the aforementioned analysis regarding fluoride removal from the PG is validated. Fig. 13 shows

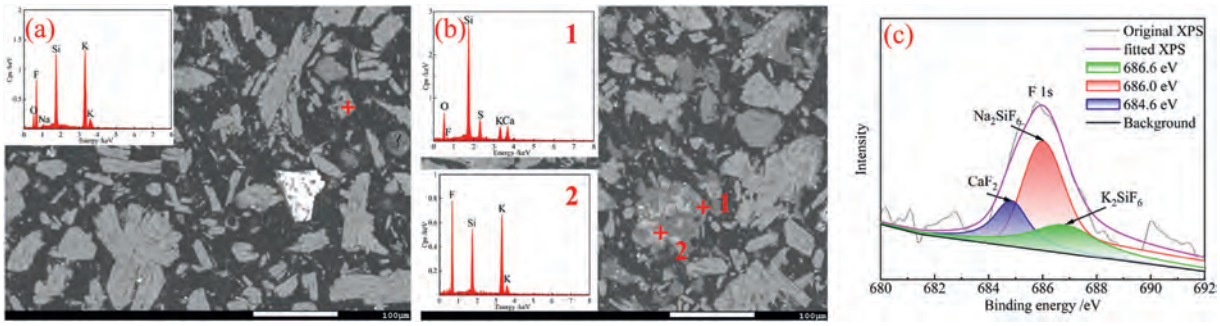

Fig. 10. Analysis of the fluorine composition in the products after a 15 min reaction: (a), (b) EBSD-EDS, (c) F 1s XPS spectra.

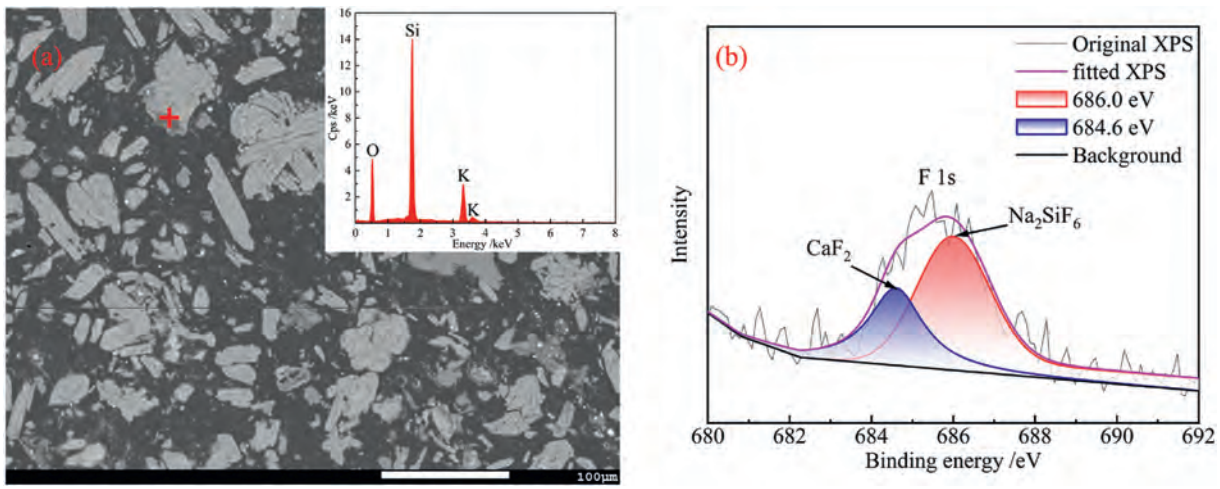

Fig. 11. Analysis of the fluorine composition in the products after a 45 min reaction: (a) EBSD-EDS, (b) F 1s XPS spectra.

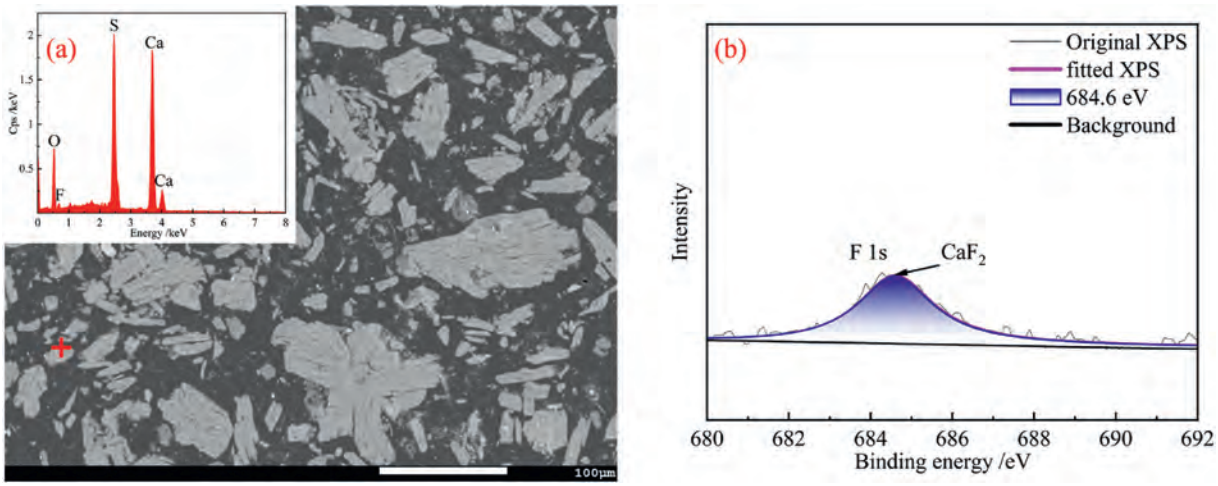

Fig. 12. Analysis of the fluorine composition in the products after a 60 min reaction: (a) EBSD-EDS, (b) F 1s XPS spectra.

the variation in the binding energies of Si, K, and Na in the PG. As shown in Fig. 13(a)–(c), the binding energies of Si 2p, K 2p and Na 1s all tend to shift towards lower values as the reaction time increases. This trend is attributed to the breakage of Si-F covalent bonds and ionic bonds between K^+/Na^+ and F^- in Na_2SiF_6 and K_2SiF_6 during the reaction, as well as the subsequent interaction of Si, K, and Na with O elements in the steam, formation Si—O covalent bonds and K^+/Na^+ and O^{2-} ionic bonds. This process ultimately leads to the formation of Na_2SiO_3 and K_2SiO_3, resulting the variation of binding energies.

3.4.3. *Mechanistic analysis*

Based on the aforementioned research findings and literature reports [25,34,35], this study proposes the following mechanism for the removal of fluorine impurities in PG.

(1) At high temperatures, $CaSO_4{\cdot}2H_2O$ undergoes dehydration, leading to the destruction of its crystalline structure. This process enables steam to penetrate the gaps between $CaSO_4$ crystals, promoting interactions with SiO_2 and fluorides such as K_2SiF_6 and Na_2SiF_6.

$$CaSO_4 \cdot 2H_2O \rightarrow CaSO_4 + 2H_2O(g) \quad (9)$$

(2) Steam ($H_2O(g)$) is initially adsorbed onto the defective silicon sites on the SiO_2 surface. With sufficient energy, $H_2O(g)$ dissociates to form hydroxyl radicals ($\cdot OH$) and hydrogen radicals ($\cdot H$) [30,36,37].

$$H_2O(g) \xrightarrow{SiO_2} \cdot OH + \cdot H \quad (10)$$

(3) OH and $\cdot H$ migrate toward the fluoro-silicate direction, disrupting its structure (The observed shift in the binding energies of Si 2p, K $2p_{3/2}$, and Na 1s toward lower values, as illustrated in Fig. 13, further supports this conclusion). In this process, the Si—F bond is cleaved, resulting in the generation of Si—OH. One portion of the liberated F^- ions combines with free $\cdot H$ radical to form an H-F bond, which then desorbs from surface of fluoro-silicate. Meanwhile, another portion of the F^- ions attacks the O—H bond from Si—O—H and leads to the formation of H—F bond. Ultimately, this leads to the formation of potassium or sodium silicate.

$$K_2SiF_6 + 3 \cdot OH + 3 \cdot H \rightarrow K_2SiO_3 + 6HF(g) \quad (11)$$

$$Na_2SiF_6 + 3 \cdot OH + 3 \cdot H \rightarrow Na_2SiO_3 + 6HF(g) \quad (12)$$

4. Conclusions

This study investigates the effect of a steam atmosphere on the removal of fluorine impurities from PG. Various characterization techniques, including EBSD-EDS, XPS, XRF, XRD, and SEM, were used to analyze the speciation of fluorine impurities in the solid phase of PG before and after the reaction, revealing their changes

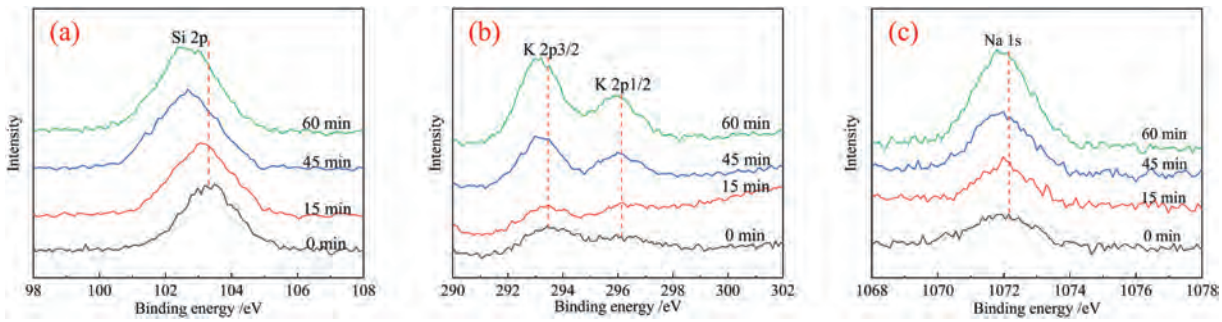

Fig. 13. XPS analysis of elements in the products under different reaction times: (a) Si 2p, (b) K 2p, (c) Na 1s XPS spectra.

and removal processes. Thermodynamic calculations were conducted to explore potential reactions involved in the defluorination process. Additionally, experimental studies assessed factors influencing fluorine removal, leading to the determination optimal process conditions. The kinetics and mechanisms of fluorine removal through thermal treatment in a steam atmosphere were also examined. Based on these investigations, the following conclusions are drawn:

(1) In PG, fluorine impurities are primarily presented as K_2SiF_6 and Na_2SiF_6, with a minor presence of CaF_2. Experimental results indicate that a steam atmosphere significantly enhances the defluorination rate of PG compared to N_2(g) and CO_2(g) atmospheres. Thermodynamic analysis, along with EBSD-EDS and XPS results, indicates that under a steam atmosphere, thermal treatment facilitates fluorine removal. CaF_2 is difficult to remove due to its high stability. K_2SiF_6 is relatively easy to eliminate, while Na_2SiF_6 is removed to a lesser extent. Moreover, most fluorine in PG is removed in the form of gaseous HF(g), facilitating subsequent recovery and utilization.
(2) The optimal process parameters for removing fluorine impurities from PG using H_2O(g) are as follow: a steam velocity of 0.0184 $m \cdot s^{-1}$, a reaction temperature of 700 °C, and a reaction time of 60 min. Under these conditions, the fluorine removal rate reaches 95.87%.
(3) Using the shrinking core model (SCM) for kinetic analysis of the fluorine removal process, the results show that defluorination of PG is controlled by internal diffusion, with an activation energy of 30.12 $kJ \cdot mol^{-1}$, which is significantly lower than that of traditional processes.
(4) The defluorination mechanism is as follows: At high temperatures, the structure of PG particles is disrupted, resulting in the formation of numerous cracks, which enhances contact between fluorides and SiO_2 with the gas phase. SiO_2 promotes the polarization of steam, leading to the formation of hydroxyl radicals (·OH) and hydrogen radicals (·H). Subsequently, ·OH breaks the Si—F bonds in fluorosilicates (K_2SiF_6 and Na_2SiF_6), resulting in the formation of Si—OH and H—F bonds. Hydrogen fluoride (HF(g)) then escapes as a gas, while the fluorosilicates transform into silicates (K_2SiO_3 and Na_2SiO_3), thereby achieving the removal of fluorine.

Overall, compared to traditional thermal treatment methods, this study reduces the reaction temperature from 950 °C to 700 °C, thereby enhancing the defluorination rate and enabling the recovery of fluoride resources. However, the method still faces the challenge of high energy consumption. To address this, future research could explore combining this approach with high-temperature decomposition processes for PG. This combination would not only facilitate the recovery of fluoride resources from PG but also promote the utilization of calcium and sulfur, contributing to the sustainable development of the phosphoric chemical industry.

CRediT Authorship Contribution Statement

Huagui Jin: Writing – original draft, Investigation, Formal analysis, Data curation, Conceptualization. Xuebin An: Writing – review & editing, Methodology, Investigation, Formal analysis, Data curation. Shizhao Wang: Project administration, Funding acquisition, Data curation. Yunshan Wang: Writing – review & editing, Supervision, Project administration, Methodology, Funding acquisition, Data curation. Gang Yang: Writing – review & editing, Project administration, Investigation, Funding acquisition, Formal analysis. Yong Sun: Writing – review & editing, Supervision, Project administration, Funding acquisition.

Declaration of Competing Interest

The authors declare that they have no known competing financial interests or personal relationships that could have appeared to influence the work reported in this paper.

Acknowledgements

This work was funded by the National Key Research and Development Program of China (2018YFC1903500),the National Key Research and Development Program of China (2019YFC1905800), Hebei Provincial Key Research Projects (22373101D) and the commercial project by Beijing Zhong Dian Hua Yuan Environment Protection Technology Co., Ltd. (E01211200005).

References

[1] D. Li, J. Jiao, D. Liao, The development and thinking of phosphogypsum used in new building materials in China, *New Building Materials* 48 (11) (2021) 1–4+11. (in Chinese)
[2] H. Deng, S. Hou, Z. Li, G. Xu, R.a. Chi, B. Xi, Update and future of phosphogypsum reuse, *Inorg Chem Industry* 56 (1) (2023) 1–8+1. (in Chinese)
[3] J. Xia, Bottleneck and key technology of phosphogypsum as building material, *Phos & Com Fert* 35 (11) (2020) 6. (in Chinese)
[4] X. Li, X.F. Lv, L. Xiang, Review of the state of impurity occurrences and impurity removal technology in phosphogypsum, *Materials* 16 (16) (2023) 5630.
[5] H.T. Zhao, H.Q. Li, W.J. Bao, C.Y. Wang, S.G. Li, W.G. Lin, Spectral analysis of trace fluorine phase in phosphogypsum, *Spectrosc. Spectr. Anal.* 35 (8) (2015) 2333–2338.
[6] C. Li, S.Z. Wang, Y.S. Wang, X.B. An, G. Yang, Y. Sun, Study on synergistic leaching of potassium and phosphorus from potassium feldspar and solid waste phosphogypsum *via* coupling reactions, *Chin. J. Chem. Eng.* 65 (2024) 117–129.
[7] D.B. Jiang, J.H. Tan, P. Yuan, H.X. Guan, P.L. Nan, Methods of the harmless treatment of harmful components in phosphogypsum, *J. Jilin Inst. Chem. Technol.* 31 (1) (2014) 33–36.
[8] F. Arianpour, A.Ç. Arianpour, B. Aali, Characterization and properties of sodium hexa-fluorosilicate and its potential application in the production of sodium fluoride, *Silicon* 13 (12) (2021) 4381–4389.
[9] W.X. Cao, W. Yi, J.H. Peng, J. Li, S.H. Yin, Recycling of phosphogypsum to prepare gypsum plaster: effect of calcination temperature, *J. Build. Eng.* 45 (2022) 103511.
[10] H.G. Jin, Y.X. Wang, X.B. An, S.Z. Wang, Y.S. Wang, G. Yang, L.F. Shi, Y. Sun, A review of fluoride removal from phosphorous gypsum: a quantitative analysis *via* a machine learning approach, *Materials* 17 (14) (2024) 3606.
[11] M. Zeng, Y. Ruan, J. Chen, C. Wang, B. Zhang, Z. Zhou, Effects Comparison of different pretreatment methods to phosphogypsum, *The World Build Mater* 32 (2) (2011) 18–21.
[12] H. Zhao, W. Bao, Z. Sun, S. Li, H. Li, W. Lin, Deep removal of impurities from phosphogypsum, *Chem. Ind. Eng. Prog.* 36 (4) (2017) 1240–1246. (in Chinese)
[13] B. Ping, H. Jun-song, L. Ao-lan, G. Hong, A review on comprehensive utilization and pretreatment method of phosphogypsum, *Mod. Chem. Ind.* 43 (S2) (2023) 76–79+85. (in Chinese)
[14] Z. Li, J. Chen, Q. Zhang, Z. Shen, A Study on the removal of phosphorus and fluorine impurities from phosphogypsum, *Acta Mineral. Sin.* 40 (5) (2020) 639–646. (in Chinese)
[15] M. Yang, Y. Pang, Investigation of cement retarder made of chemically pretreated phosphogypsum, *J. Lanzhou Univ. Technol.* 33 (6) (2007) 58–60.
[16] Y. Ennaciri, I. Zdah, H. El Alaoui-Belghiti, M. Bettach, Characterization and purification of waste phosphogypsum to make it suitable for use in the plaster and the cement industry, *Chem. Eng. Commun.* 207 (3) (2020) 382–392.
[17] L. Zou, The Effect of Additives on the Crystallzation Process of Calcium Sulfate, Master Thesis, Tianjin University of Science and Technology, Tianjin, 2000.
[18] Q. Fu, S. Luo, X. Ma, X. Wang, Z. Zhang, X. Wang, L. Yang, Impurities removal from phosphogypsum by leaching neutralization method, *Inorg. Chem. Indust.* 47 (7) (2015) 44–47. (in Chinese)
[19] M.M. Smadi, R.H. Haddad, A.M. Akour, Potential use of phosphogypsum in concrete, *Cement Concr. Res.* 29 (9) (1999) 1419–1425.
[20] T.Y. Ren, J. Zhu, W.C. Liu, X.F. Zhu, J.K. Yang, Water resistance of composite binders containing phosphogpysum with different pretreatment processes, *Adv. Cement Res.* 24 (2) (2012) 111–120.
[21] F. Pan, S.G. Ma, Y. Ge, C.L. Fan, Q.S. Zhu, Fluidization thermal decomposition of sodium fluosilicate, *Chin. J. Chem. Eng.* 57 (2023) 329–337.

[22] V.S. Singh, S.V. Moharil, Synthesis and characterization of K_2SiF_6 hexafluorosilicate, *IOP Conf. Ser. Mater. Sci. Eng.* 1104 (1) (2021) 012004.
[23] N. Soltani, M.I. Pech-Canul, L.A. González, A. Bahrami, Mechanism and parameters controlling the decomposition kinetics of Na_2SiF_6 powder to SiF_4, *Int. J. Chem. Kinet.* 48 (7) (2016) 379–395.
[24] R. Stodolski, L. Kolditz, Some aspects of real structure and thermal decomposition of K_2SiF6, *J. Fluor. Chem.* 29 (1–2) (1985) 73.
[25] C. Liu, J.X. Gu, S. Zhou, B.B. Qian, B. Etschmann, J.Z. Liu, D.X. Yu, L. Zhang, Silica-assisted pyro-hydrolysis of $CaCl_2$ waste for the recovery of hydrochloric acid (HCl): reaction pathways with the evolution of Ca(OH)Cl intermediate by experimental investigation and DFT modelling, *J. Hazard Mater.* 439 (2022) 129620.
[26] C. Liu, J. Gu, S. Zhou, B. Qian, B. Etschmann, J.Z. Liu, D. Yu, L. Zhang, Silica-assisted pyro-hydrolysis of $CaCl_2$ waste for the recovery of hydrochloric acid (HCl): reaction pathways with the evolution of Ca(OH)Cl intermediate by experimental investigation and DFT modelling, *J. Hazard Mater.* 439 (2022) 129620.
[27] Y.J. Liu, The detemination of fluorine content in ground phosphate rock, *J. Shenyang Norm. Univ. Nat. Sci.* 20 (2) (2002) 124–127.
[28] Y. Kashiwaya, A.W. Cramb, Kinetics of formation and dissociation of Na_2SiF_6, *Metall. Mater. Trans. B* 33 (1) (2002) 129–136.
[29] Y. Sun, V. Sage, Z. Sun, An enhanced process of using direct fluidized bed calcination of shrimp shell for biodiesel catalyst preparation, *Chem. Eng. Res. Des.* 126 (2017) 142–152.
[30] Y.S. Wang, L.F. Shi, H.L. Li, Y.X. Wang, Z.Y. Wang, X.B. An, M.Z. Tang, G. Yang, J. He, J. Hu, Y. Sun, Clean process to utilize the potassium-containing phosphorous rock with simultaneous HCl and KCl production *via* the steam-mediated reactions, *ACS Omega* 7 (28) (2022) 24561–24573.
[31] Q. Qi, J. Liu, X. Cao, J. Zhou, S. Zhang, K. Cen, Stability of CaF_2 at high temperature, *Environ. Sci.* 23 (3) (2002) 111–114. (in Chinese)
[32] D.L. Deadmore, J.S. Machin, A.W. Allen, Stability of inorganic fluorine-bearing compounds: I, binary metallic fluorides, *J. Am. Ceram. Soc.* 44 (3) (1961) 105–109.
[33] D.L. Deadmore, J.S. Machin, A.W. Allen, Stability of inorganic fluorine-bearing compounds: II, complex fluorides, *J. Am. Ceram. Soc.* 45 (3) (1962) 120–122.
[34] M. Kanezashi, T. Matsutani, H. Nagasawa, T. Tsuru, Fluorine-induced microporous silica membranes: dramatic improvement in hydrothermal stability and pore size controllability for highly permeable propylene/propane separation, *J. Membr. Sci.* 549 (2018) 111–119.
[35] F.L. Liu, Y.Y. Chen, B. Milićević, C.Y. Jiang, S.C. Huang, L. Zhou, J.B. Zhou, M.M. Wu, Hydroquinone-modified Mn^{4+}-activated fluoride red phosphors with improved water-resistance, *Colloids Surf. A Physicochem. Eng. Aspects* 661 (2023) 130954.
[36] J. Yeon, Development of a reaxff reactive force field for silicon/oxygen/hydrogen/fluoride interactions and applications to hydroxylation and friction, Ph. D. Thesis, The Pennsylvania State Univ., USA, 2016.
[37] Y. Xia, J. Li, Y.Z. Zhang, Y.G. Yin, B.L. Chen, Y. Liang, G.B. Jiang, R.N. Zare, Contact between water vapor and silicate surface causes abiotic formation of reactive oxygen species in an anoxic atmosphere, *Proc. Natl. Acad. Sci. USA* 120 (30) (2023) e2302014120.